Journal of Materials Chemistry A

Accepted Manuscript

ROYAL SOCIETY OF CHEMISTRY

www.rsc.org/materialsA

Journal of Materials Chemistry A RSCPublishing

ARTICLE

Transparent, Thermally and Mechanically Stable Superhydrophobic Coating Prepared by Electrochemical Template strategy

Lianyi Xu, Dandan Zhu, Xuemin Lu, and Qinghua Lu*

Cite this: DOI: 10.1039/xoxxoooooox

Received ooth January 2012,
Accepted ooth January 2012

DOI: 10.1039/xoxxoooooox

www.rsc.org/

By mimicking nature, the preparation of artificial self-cleaning surfaces has gradually matured both in theory and technology, but its actual application has been hampered by enormous difficulties. The main challenge is that its design principle (i.e., its requirement for micro- and nano-structures) is difficult to reconcile with the need for coating strength and transparency. Here, we have exploited a porous structured silica coating with the help of an electrodeposited porous PEDOT template. This porous silica coating not only provides the requisite roughness for the final superhydrophobic surface, but also has a low refractive index, thereby enhancing the transparency of the silica coating. After fluorination, a highly transparent, thermally and mechanically stable superhydrophobic coating was obtained. The silica coating enables to withstand tests of harsh environments, such as mechanical resistance and ultra-high hydraulic pressure tests. This large-area superhydrophobic coating has great potential for use in solar cells and self-cleaning windows.

Introduction

There is ever-growing interest in the fabrication of superhydrophobic non-adhesive surfaces.[1–6] These surfaces display an apparent water contact angle greater than 150°, and water droplets dropped onto them at a small tilt angle can automatically roll off with contaminants and dust. Such surfaces have great potential applications in many fields, such as self-cleaning coatings, anti-fouling surfaces, microfluidics, and oil-water separation.[1] Nevertheless, the structured surfaces also have inherent drawbacks, such as a propensity to lose their self-cleaning properties, especially when they are subjected to external pressure, impact, or poor environments.[7–8] In addition, the non-transparency of the majority of self-cleaning coatings also limits their applications in solar cells, car windshields, and display windows.[9–13] Although many groups have made great efforts to enhance the thermal and mechanical stability, pressure resistance, and transparency of artificial superhydrophobic surfaces,[7–8] no perfect technique has yet been devised to achieve simultaneously transparent and abrasion-resistant superhydrophobic surfaces.[12,13] The main challenge is that it is difficult to reconcile the required coating characteristics. For example, reducing rough surface structure dimension to avoid light scattering, thus improving the transparency of coatings, often causes a loss of self-cleaning and anti-adhesion properties, and vice versa.[12] Besides, the surface rough structures formed by nanoparticle assemblies and hybrid composites may give rise to poor mechanical stability due to the weak interaction between particles and matrix/substrate, such that the films are more readily destroyed under extreme conditions.[11–13] Thus, as yet, the actual application of such coatings is still hampered.

Here, in contrast to the usual design concept for transparent superhydrophobic coatings, we have exploited an in situ formed nanostructured silica coating, which not only provide a mechanically stable rough structure for superhydrophobic coating, but also enhance its transparency.[14] This idea for such a silica grew out of the inspiration from the electrodeposited poly(3,4-ethylenedioxythiophene) (PEDOT) film, which has the highly porous network-like nanostructure and good transparency. Based on the understanding of its surface characterizations, we propose a novel and simple approach for the large-area and low-cost preparation of transparent, thermally and mechanically stable superhydrophobic coatings. Firstly, the porous network-like PEDOT film was electrodeposited on a large-area indium tin oxide (ITO) glass electrode (Scheme 1); this PEDOT film as a nanostructure template was then covered by a silica layer by chemical vapor deposition (CVD) of tetraethoxysilane (TEOS) for 30 h in the presence of ammonia.[9] After removing the PEDOT by annealing at 500 °C for 2 h in air, a transparent and superhydrophilic silica coating was obtained. Finally, through the deposition of 1H,1H,2H,2H-perfluorooctyltriethoxysilane (POTS) on the superhydrophilic silica coating, a transparent superhydrophobic non-adhesive surface, and even a superoleophobic surface, could be achieved. The transparency, thermal and mechanical stabilities, and pressure resistance of the coating were further investigated.

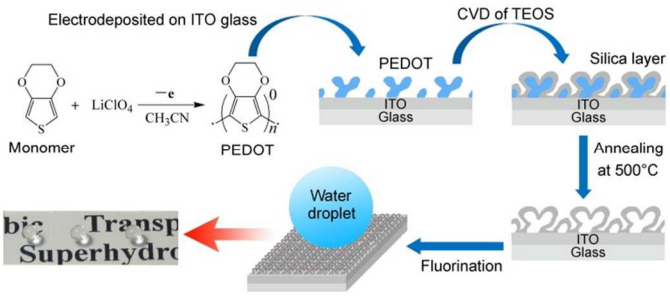

Scheme 1. The procedure for preparing a transparent, superhydrophobic porous silica coating by using an electrodeposited poly(3,4-ethylenedioxythiophene) (PEDOT) film as a template.

Experimental

Materials

HPLC grade acetonitrile (ACN) was provided by Shanghai Lingfeng Chemical Reagent Company. 3,4-Ethylenedioxythiophene (EDOT) (Adamas, 99%), tetraethoxysilane (TEOS) (Aladdin, 98%), ammonia solution (Aladdin, 25–28%), 1H,1H,2H,2H-perfluorooctyltriethoxysilane (POTS) (Alfa Aesar, 97%), hexadecane (Adamas, 98%), peanut oil (commercial), ethylene glycol (Adamas, 99%), diiodomethane (Adamas, 97%), and anhydrous lithium perchlorate ($LiClO_4$) (J&K, 99%) were used directly without further purification.

Preparation of PEDOT films

Electrochemical preparation of PEDOT films was performed in a three-electrode electrochemical cell by using a computer-controlled CHI 630E Electrochemical Analyzer (Figure S1a). In this electrochemical system, ITO glass (<10 Ω sq^{-1}, 0.9 cm× 5 cm), platinum wire (1 mm diameter), and Ag/AgCl wire were used as working-, counter-, and quasi-reference electrode, respectively. ITO galss was washed successively under ultrasonication with deionized water and absolute ethanol, and then dried with a stream of N_2 before use. For the preparation of the large-area PEDOT film (about 10 × 8 cm^2), the stainless steel sheet electrode with an area of about 11 × 11 cm^2 was used as counter-electrode. Before the electrochemical experiment, the stainless steel sheet was cleaned successively with 1 M NaOH solution and absolute ethanol, and activated by using 1 M hydrochloric acid for about 5 min, and then cleaned with deionized water, dried in air. The electrochemical experiments were performed at room temperature and less than 40% relative humidity. PEDOT was electrodeposited on ITO electrodes by cyclic voltammetry (CV) between −0.8 V and +1.5 V in 0.01 M EDOT/ACN solution containing 0.2 M $LiClO_4$ as a supporting electrolyte (Figure 1a). The as-prepared PEDOT films were rinsed three times with ethanol (95%) and dried under an air stream at room temperature.

Preparation of Silica coatings

PEDOT films were placed in a closed desiccator together with two open vessels containing about 2 ml of tetraethoxysilane (TEOS) and 1ml of aqueous ammonia solution, respectively. The chemical vapor deposition (CVD) of TEOS was performed at room temperature for 30 hours. Then the silica-layer-encased PEDOT films were calcinated at 500 °C for 2 h in air to remove PEDOT templates. Finally, the as-prepared superhydrophilic silica coatings were fluorinated by preforming CVD of 1H,1H,2H,2H-Perfluorooctyltriethoxysilane (POTS) at room temperature for 12 hours in a similar device mentioned above.

Measurement of contact angles

Static contact angle (CA) measurements in air were performed by the sessile drop method using an OCA 20 contact angle system (Data Physics Instruments GmbH, Germany). The reported CAs are the mean values of measurements on a 4 μL water droplet or 5 μL organic droplet at three different positions on each sample. Sliding angles (SA), advancing angles (θ_A), and receding angles (θ_R) were determined by slowly tilting the sample stage until the 4 μL water droplet or 5 μL organic droplet started to move.

Characterization

Field-emission scanning electron microscopy (FE-SEM) was performed with a Nova NanoSEM instrument (FEI, U.S.A.). The high-speed video and sequential photography images of impacting water-droplet on the coating were captured at 1200 fps using a high-speed camera (Motion Studio Cameras SDK, IDT, Inc.) The chemical compositions of the surfaces were determined by XPS on a Kratos Axis Ultra^{DLD} spectrometer (Kratos Analytical, Ltd., Manchester, U.K.) using monochromatic Al-K_α radiation (1486.6 eV) and a takeoff angle of 90°. Transmittance measurements were performed using a Perkin-Elmer Lambda 20 UV/Vis spectrophotometer in double-beam mode. Refractive index and coating thickness were measured using W-VASE on an AutoRetarder^{TM} variable-angle spectroscopic ellipsometer (J.A. Woollam, U.S.A.). Reflectance measurements were made on a Perkin-Elmer Lambda 950 UV/Vis spectrometer with a 150 mm integrating sphere. Photographs were acquired with a camera.

Results and discussion

Electrochemical preparation and morphology

Electrochemical deposition technique provides a facile and controllable way to prepare rapidly the large-area π-conjugated polymer films.[15,16] PEDOT, as an important π-conjugated polymer, was easily electrodeposited on large-area ITO glass by cyclic voltammetry (CV) (for about 60 s) in a monomer-containing $LiClO_4$/acetonitrile (ACN) solution (see CV curve in Figure 1a, Figure S1a). Here, the resulting PEDOT film not only possessed a highly porous network-like nanometer structure (Figure 1b), but also exhibited a blue-transparent and superhydrophilic surface (WCA ≈ 0°) due to its capillary effect (inset in Figure 1b, Figure S1b). Figure 1c was the scanning electron microscope (SEM) image of the PEDOT film encapsulated in silica layer (*e.g.* PEDOT/silica hybrid bilayer film), and the bilayer structure still remained porous even after 30 h of CVD of TEOS. For the creation of a colorless, transparent silica coating, the PEDOT was removed from the PEDOT/silica hybrid bilayer film by calcination in air. The resulting silica coating retained its highly porous rough structure with dimension less than 500 nm (Figure 1d). The cross-sectional image of the silica coating shows a lot of irregular holes that were initially filled with PEDOT polymer (inset in Figure 1d).

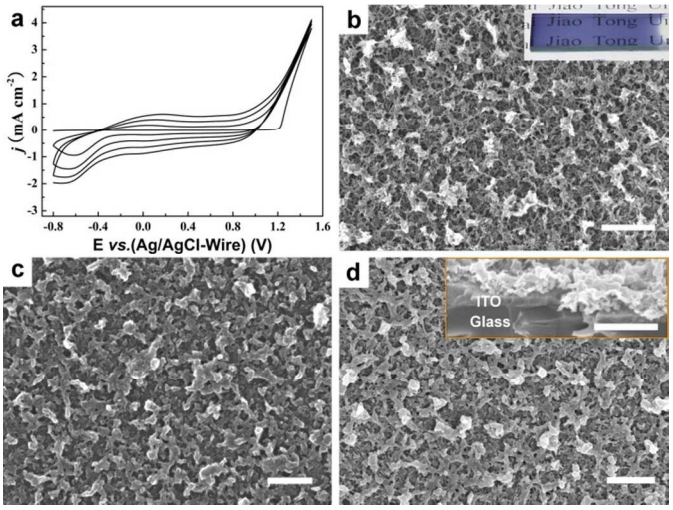

Figure 1. (a) Successive CV curves of the electrodeposition of PEDOT on the ITO substrate. (b) SEM image of the highly porous network-like PEDOT film. Inset: Photograph of PEDOT film electrodeposited on ITO glass. (c) SEM image of PEDOT film coated with a silica layer by CVD of TEOS. (d) SEM image of the porous silica coating obtained after removing the PEDOT template by calcination in air. Inset: oblique view of the cross-sectional silica coating showing the unique inner hollow structure. All scale bars represent 1 μm.

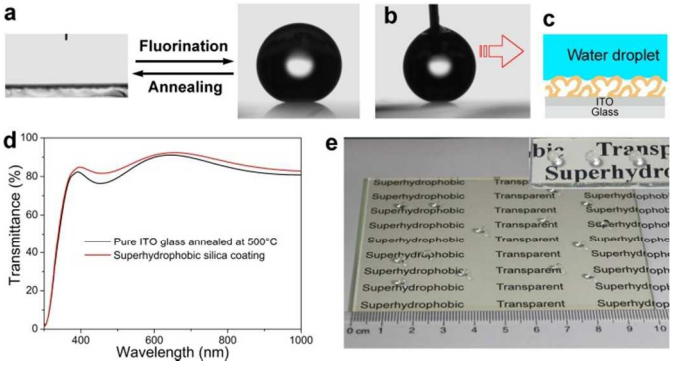

Figure 2. (a) The resulting silica coating can be transformed between superhydrophilicity (WCA ~ 0°, left) and superhydrophobicity (WCA ~ 168.0, right). (b) Lateral movement of the water droplet hanging at the tip of a needle on the superhydrophobic coating surface. (c) Schematic representation of the solid/liquid/air three-phase contact line on the fluorinated silica layer (Cassie state). (d) UV/Vis transmittance spectra of the superhydrophobic silica coating (red line), and of pure ITO glass annealed at 500 °C in air for 2 h (black line). (e) Photograph of many randomly distributed water droplets (8 μL) deposited on the large-area transparent superhydrophobic silica coating (about 10 × 8 cm^2). The silica-coated ITO glass was placed on the labeled paper. Inset: the magnified photograph of water droplets (4 μL) on the transparent superhydrophobic silica coating.

Superhydrophobicity

The resulting silica coating displayed transparency and superhydrophilic property (Figure 2a (left)). The silica coating was further coated with POTS by CVD under catalysis by ammonia. After 12 h, a superhydrophobic surface was obtained, on which a water droplet (4 μL) exhibited a static water contact angle of 168.0° ± 1° and a sliding angle smaller than 2° (Figure 2a (right)). The water contact angle hysteresis (ΔH) was 5.5° ± 1° (advancing angle $\theta_A \approx 168.2° \pm 1°$; receding angle $\theta_R \approx 162.7° \pm 1°$; $\Delta H = \theta_A - \theta_R$). This low ΔH derives from a non-adhesive superhydrophobic surface, as evidenced further by the nearly friction-free lateral movement of a 4 μL water droplet hanging at the tip of a needle on such a surface (Figure 2b and Movie S1). These evidences suggest that the behavior of water droplet on the highly porous superhydrophobic coating follows the Cassie-Baxter model,[3,5] which describes that the liquid droplet is sitting on top of the hierarchical rough surface with air pockets remaining trapped beneath the liquid droplet, leading to a composite liquid-solid-air contact interface (Figure 2c). The wetting transition from superhydrophilicity to non-adhesive superhydrophobicity can be attributed to the successful introduction of the low-surface-energy fluorosilane, as evidenced by the strong F1s peak at 691.8 eV in the X-ray photoelectron spectrum (Figure S2).

Transparency

Compared to traditional particle–hybrid superhydrophobic coatings, such a highly porous nanostructure is beneficial for reducing the scattering of propagated light, improving the transparency of the silica coating.[12] As evidenced by UV/Vis transmittance spectra (Figure 2d (red), Figure S3), the superhydrophobic non-adhesive coating is transparent. The superhydrophobic silica coating (such as that obtained with an electrodeposition charge (EC) of 14.8 mC cm^{-2} for the PEDOT template) showed more than 81.7% transmittance for wavelengths above 374 nm, and even showed 92.8% transmittance at 661 nm. The good transparency of the resulting large-area superhydrophobic coating (about 10 × 8 cm^2) could be more directly proved by showing the clarity of letters beneath the silica-coated ITO glass substrate (Figure 2e). Many randomly distributed water droplets (8 μL) on such transparent coating showed nearly spherical shape, further indicating its good superhydrophobicit property (the fluorinated ITO surface without porous structure only showed a water contact angle (WCA) of 111.2° ± 1°, see Figure S4a). Notably, the transmittance of the silica coating is better than that of the pure ITO glass (annealed at 500 °C in air for 2 h) in the long-wavelength range from 368 nm to more than 1000 nm (Figure 2d, Figure S3). This result means that the porous nanostructured silica coating enhanced the transparency of its ITO glass substrate (see photograph in Figure S4b), which may be attributed to the reducion of surface reflection.[14]

Tunable superhydrophobicity and transparency

The superhydrophobicity of the silica coating is also related to the electrodeposition charge (EC) of the PEDOT template. Here, silica coatings with EC of 7.5, 10.5, 17.8, 23.9, 29.9, 35.3, 43.5, and 56.7 mC cm^{-2} (denoted as C1 to C8, respectively) were investigated. As shown in Figure 3a, all of the silica

coatings displayed superhydrophobicity with a low sliding angle (non-adhesion), apart from coating C1, which exhibited a high-adhesion superhydrophobic surface (see inset in Figure 3a). The difference of the superhydrophobicity should be attributed to the thickness of the porous silica caused by the thickness of the template PEDOT. A thin PEDOT template obtained with EC less than 10.5 mC cm^{-2} is unfavorable for preparing a Cassie superhydrophobic surface. On the contrary, when the EC of the PEDOT template exceeded 56.7 mC cm^{-2}, the PEDOT film was exfoliated too readily, so that the template did not fit to make a high-quality silica coating on the ITO glass. Therefore, superhydrophobic coatings showing both the pinned and sliding superhydrophobic states can be achieved by altering the EC of the template. The adhesive-tunable superhydrophobic coating maybe have a good use in ultra-low-loss micro-droplet transport, micro-fluid control systems , solar cells and self-cleaning windows (see inset in Figure 3a, Figure S4c).[6]

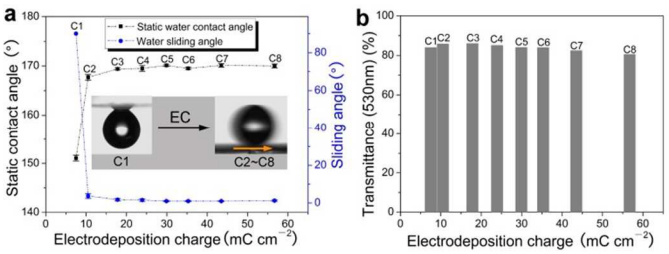

Figure 3. (a) The effect of the electrodeposition charge (C1 to C8, respectively) of the PEDOT templates on WCA and SA of the final superhydrophobic silica coatings. Inset: the tunable adhesion of water droplet between the pinned (C1) and sliding (C2 to C8) superhydrophobic state. (b) The effect of the electrodeposition charge of the PEDOT templates on the transmittance (at 530 nm) of the final superhydrophobic coatings (C1 to C8).

Interestingly, according to the UV/Vis spectra, all of these silica coatings showed more than 80.5% transmittance at 530 nm (83.9% (C1), 85.8% (C2), 86% (C3), 85.1% (C4), 84.0% (C5), 83.9% (C6), 82.4% (C7), and 80.5% (C8), respectively; the annealed pure ITO glass as a control showed 83.1% transmittance) (Figure 3b). The coating C3 showed the highest transmittance; thereafter, the transmittances of the coatings at 530 nm slowly decreased with the EC of the PEDOT templates (Figure 3b, Figure S5), but such a small change is almost impossible to distinguish by showing printed letters under these superhydrophobic fluorinated silica-coated ITO glasses (Figure S6). These results indicate that the transparent superhydrophobic silica coatings can be readily produced over a wide range of electrodeposition charges from 10.53 to 56.7 mC cm^{-2}.

Oil repellency

The transparent silica coating (EC of 47.7 mC cm^{-2} for PEDOT) not only showed super water-repellency, but also oil repellency with static contact angles ranging from 128.6° ± 4° for hexadecane (5 μL) up to 161.1° ± 2° for diiodomethane (5 μL) (Figure 4a, Table 1). Especially, the silica coating presents the low adhesion for diiodomethane with a SA of 4° ± 2° and for ethylene glycol with a SA of 6° ± 2°. As shown in Figure 4b, the nearly spherical organic droplets of diiodomethane, ethylene glycol and peanut oil on the transparent silica coating can be clearly observed. Furthermore, the oleophobicity of the coating was also found to depend on the EC of the PEDOT templates (Figure 4c, for diiodomethane). The properties can be attributed to the unique porous nanostructured morphology of the silica coating.[3,17] Although superoleophobicity was only seen for some organic solvents with lower surface tension, the idea opens a door for the design of both superhydrophobic and superoleophobic transparent surfaces, which is of great significance for practical applications to maintain the self-cleaning property of the coatings.[9]

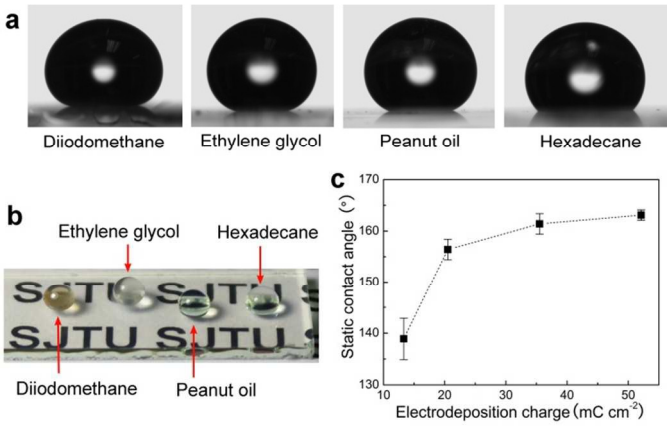

Figure 4. (a) CA measurements of organic liquids (5 μL): diiodomethane with CA of 161.1° ± 2°, ethylene glycol with CA of 159.4° ± 2°, peanut oil with CA of 150.7° ± 3°, and hexadecane with CA of 128.6° ± 4°. (b) Photograph of organic droplets (5 μL) deposited on the transparent silica-coated ITO glass. (c) The effect of the EC of the PEDOT templates on the oleophobicity of the silica coating (for diiodomethane).

Table 1. Comparison of the static contact angles (CA) and sliding angles (SA) of organic drops (5 μL) with different surface tensions, deposited on a flat fluorinated ITO glass surface and on a superhydrophobic silica-coated ITO glass surface with EC of the PEDOT at 47.7 mC cm^{-2}.

Organic Liquid	Surface tension [mN m^{-1}]	Flat surface [CA°]	Coated surface [CA°]	Sliding angle [SA°]
Diiodomethane	50.0	101.1 ± 2	161.1 ± 2	4 ± 2
Ethylene glycol	47.7	93.2 ± 2	159.4 ± 2	6 ± 2
Peanut oil	35.2	78.7 ± 3	150.7 ± 3	Adhesion
Hexadecane	27.5	71.8 ± 3	128.6 ± 4	Adhesion

Water-droplet impact resistance

For real applications in outdoor environments, the transparent superhydrophobic non-adhesive coating must withstand rain impact, high temperatures, and mechanical abrasion. In our work, water-droplet impact experiment was firstly performed and the impingement process of water droplets on the surface was captured by a high-speed camera. The impinging water droplet (22 μL) with a velocity of 0.75 can completely bounce off the superhydrophobic silica coating, leaving the surface dry (Figure 5a, Movie S2). Even if the water droplet impacts the surface with a higher velocity of 4.43 m s^{-1}, the coating still keeps its non-adhesion superhydrophobic surface (Figure S7a, Movie S3). Furthermore, the hydrophilic sand contaminants on such a coating could be removed easily

by the impinging water droplet, showing a self-cleaning property (Figuer 5b, Movie S4).

The durability of the superhydrophobic silica coating was also assessed by the long-term water-drop impact experiment. The tilted 45-degree silica coating (made by PEDOT's EC of 41.0 mC cm^{-2}) could keep its superhydrophobicity with a water CA of 162.5° ± 1°, after impacting of water drops (50 μL, radius of 2.3 mm) from 12 cm height (its impact velocity of about 1.53 m s^{-1}) with a dropping rate of 2 droplets per second for 24 hours (Figure S7b).

Thermal stability

The thermal stability of our superhydrophobic silica coatings was also evaluated. After annealing the transparent porous silica coating at various selected temperatures between 22 and 400 °C for 1 h each in air, the water contact angle and sliding angle thereon remained constant (Figure 5c), indicating excellent thermal stability of the transparent superhydrophobic coating. However, the silica coating lost its superhydrophobicity and became superhydrophilic after annealing at more than 400 °C owing to thermal decomposition of the fluorosilane.[9,10] If the film was further coated with POTS by CVD, its superhydrophobicity was restored (Figure 2a).

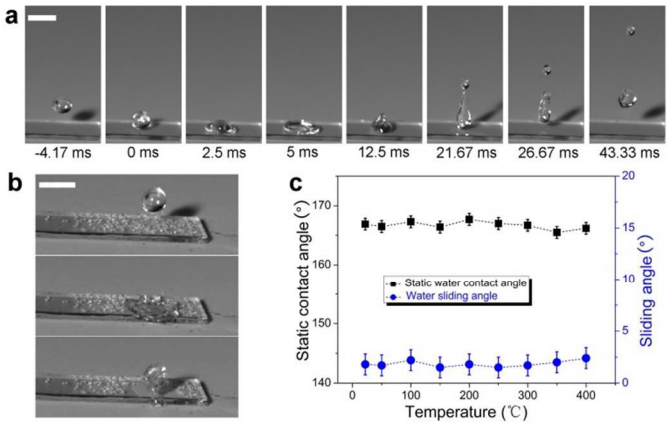

Figure 5. (a) Sequential photography images of a 22 μL water droplet bouncing off the porous superhydrophobic silica coating with an impacting velocity of 0.75 m s^{-1}. The scale bars represent 5 mm. (b) The self-cleaning property evaluated by water-droplet impact on the superhydrophobic coating. The scale bars represent 5 mm. (c) Thermal stability of a superhydrophobic silica coating evaluated by measuring its WCA and SA after annealing for 1 h at different temperatures between 22 and 400 °C.

Tape peeling test

A tape peeling test was performed to assess the adhesion between the silica coatings and ITO substrate. Double-sided sticky tape was pressed at about 100 kPa onto the silica coating (EC of the PEDOT: 15.2 mC cm^{-2}). After peeling off the tape and successively washing the surface with toluene, dichloromethane, and ethanol, we found that the porous silica coating beneath the tape stayed in place very well without any obvious damage (Figure 6a). On the contrary, after peeling off the tape, bulk adhesive remained on the surface of the silica coating if no washing (Figure S8). This indicated that the silica layer adhered firmly to the ITO substrate, rather than merely being adsorbed by van der Waals interaction, which may be due to chemical reaction between the porous silica and ITO glass substrate during annealing at high temperature to remove the PEDOT template. This mechanical stability was further verified by the fact that the superhydrophobicity (water CA of 158.5° ± 2°) was still maintained after twice tape peeling-off tests (see inset in Figure 6a).

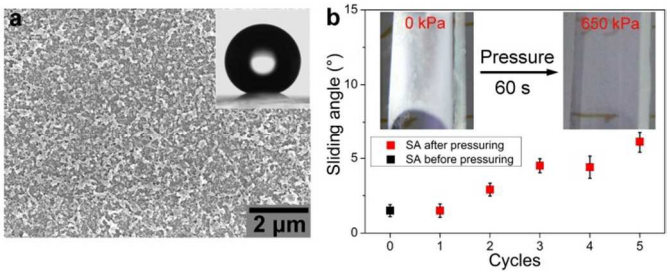

Figure 6. (a) SEM image of the superhydrophobic silica coating obtained after peeling off double-sided sticky tape and successively washing with toluene, dichloromethane, and ethanol. Inset: WCA of this coating was about 158.5° ± 2°. (b) Water SAs measured after releasing the 650 kPa pressure and removing the coating from the water without any drying process. Inset: photographs of the mirror effect of the superhydrophobic silica coating under water at applied pressures of 0 kPa (left) and 650 kPa (right).

Hydraulic pressure resistance

When a superhydrophobic coating under water was subjected to a hydraulic pressure (P_w) greater than its critical transition pressure (*Pc*), a Cassie-to-Wenzel transition can occur due to the rough structure being impregnated by water.[10,18a] In that case, such a coating would lose its self-cleaning property. Thus, for practical applications, the *Pc* of a superhydrophobic coating must be high enough to maintain its superhydrophobicity. In our work, the stability of the superhydrophobicity towards the hydraulic pressure P_w was also investigated through immersing the superhydrophobic silica coating in water with a P_w of 650 kPa for 60 s (for a diagram of the device, see Figure S9a). Before applying pressure, such a coating under water (at a depth of about 0.5 cm) can form a reflective interface like a mirror (see inset in Figure 6b (left)) due to the presence of lots of air pockets tapped by water. If a 4 μL air bubble was injected on such a coating surface, it could rapidly spread into the surface, presenting a super-aerophily (Figure S9b). When applying 650 kPa pressure for 60 s, the mirror-like reflective interface significantly faded on observing it with the naked eye (see inset in Figure 6b (right)). However, interestingly, after releasing the pressure P_w and removing the coating from the water, we found that such a coating enables automatic recovery of its initial Cassie superhydrophobic state, as evidenced by its water sliding angle of < 2° (Figure 6b). Furthermore, such a low water sliding angle (< 10°) can be maintained after subjected to five times hydraulic pressure tests (Figure 6b). The high hydraulic pressure resistance of the silica coating could be attributed to its high enough capillary pressure ($P_{capillary}$) generated within its porous hierarchical nanostructure, which can effectively balance the P_w and prevent the impregnation of water into deep pores.[8b,10,18] The evidence indicates that the resultant transparent superhydrophobic coating processes an ultra-high critical transition pressure *Pc* (a Cassie-to-Wenzel transition). This is of the utmost importance for the transparent superhydrophobic coatings out of door to resist the 10 ~ 100 kPa impact pressure of rain drops.[10,18]

Sand-abraded resistance

In the real environment, the superhydrophobic coating often is subjected to the mechanical abrasion, which leads to the loss of its superhydrophobicity. The sand abrasion test was performed by impacting of the 20 g sand grains with the diameter of 150 ± 100 μm from a height of 20 cm onto the tilted 45-degree silica coating (Figure 7a). The silica coating can keep its superhydrophobicity with water CA of 153.2° ± 2° after about 50 second sand abrasion, although some nanostructures of the silica coatings have been worn off by the sand grains (Figure 7b, Movie S5). The tests results indicated that the special nanostructure of silica coating could efficiently withstand the external impact to some extent, maintain its superhydrophobicity.

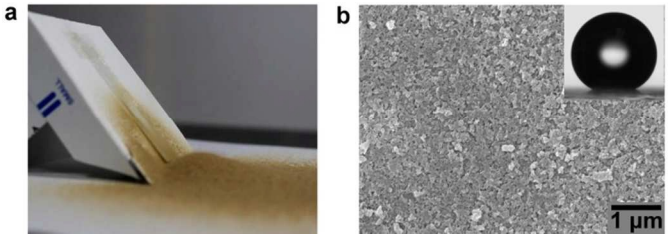

Figure 7. (a) Photograph of the sand grains abrading the tilted 45-degree superhydrophobic silica coating from an impact height of 20 cm. (b) SEM image of the superhydrophobic silica coating obtained after abraded by sand grains for about 50 s. Inset: WCA of the abraded coating was about 153.2° ± 2°.

Conclusions

In conclusion, we developed an electrochemical template strategy for the in situ preparation of a good transparent, thermally and mechanically stable superhydrophobic coating. This coating is derived from highly porous network-like PEDOT film electrodeposited ITO electrode, and the silica layer inherits a porous nanostructure from the PEDOT film. After fluorination, it displays a static water contact angle of 168.0° ± 1° and a low sliding angle (< 2°). The porous nanostructure reduces the refractive index of the silica coating, leading to a higher transparency with even 92.8% transmittance at 661 nm than that of ITO glass. The silica coating was found to withstand the harsh environment tests. The coating can keep its non-adhesion surface when subjected to the water-droplet impact with an impacting velocity of up to 4.43 m s^{-1}. Its superhydrophobicity remained unchanged after submitting it to a high temperature of up to 400 °C for 1 h. The coatings also showed excellent mechanical resistance due to the porous silica and ITO glass substrate sintering together during the annealing process of the coating to remove PEDOT. When subjected to a hydraulic pressure of up to 650 kPa, the coating could still automatically recover its superhydrophobicity after taking it out from water. The sand abrasion test was also performed to assess the abrasion resistance of the superhydrophobic coating. The transparent, thermally and mechanically stable superhydrophobic silica coating presents the immense potential applications in solar cells and self-cleaning windows. This electrochemical template preparation approach may also be extended to other conductive substrates, such as metal mesh for oil-water separation or metal plates for metal corrosion protection, and so on.

Acknowledgements

This work was supported by 973 Projects (2012CB933803, 2014CB643605), the National Science Fund for Distinguished Young Scholars (50925310), the National Science Foundation of China (21374060, 51173103), and Excellent Academic Leaders of Shanghai (11XD1403000).

Notes and references

Lianyi Xu, Dandan Zhu,Xuemin Lu, and Qinghua Lu*
School of Chemistry and Chemical Engineering, State Key Laboratory of Metal Matrix Composite, Shanghai Jiao Tong University, 800 Dongchuan Road, Shanghai, 200240, People's Republic of China
E-mail: qhlu@sjtu.edu.cn

Electronic Supplementary Information (ESI) available: [details of any supplementary information available should be included here]. See DOI: 10.1039/b000000x/

1 a) K. S. Liu, L. Jiang, Annu. Rev. Mater. Res., 2012, 42, 231; b) W. Barthlott, C. Neinhuis, Planta, 1997, 202, 1; (c) B. N. Sahoo, B. Kandasubramanian, RSC Adv., 2014, 4, 22053.

2 a) Y. K. Lai, F. Pan, C. Xu, H. Fuchs, L. F. Chi, *Adv. Mater*., 2013, **25**, 1682; b) M. J. Cheng, Q. Liu, G. N. Ju, Y. J. Zhang, L. Jiang, F. Shi, *Adv. Mater*., 2014, **26**, 306; c) Q. F Cheng, M. Z. Li, F. Yang, M. J. Liu, L. Li, S. T Wang. L. Jiang, *Soft Matter*, 2012, **8**, 6740–6743.

3 A. Tuteja, W. Choi, M. Ma, J. M. Mabry, S. A. Mazzella, G. C. Rutledge, G. H. McKinley, R. E. Cohen, *Science*, 2007, **318**, 1618; (b) J. Xiong, S. N. Das, B. Shin, J. P. Kar, J. H. Choi, J. –M. Myoung, J. Colloid Interf. Sci., 2010, **350**, 344.

4 a) Y. Li, L. Li, J. Q. Sun, *Angew. Chem.*, 2010, **122**, 6265; b) T. Darmanin, E. T. de Givenchy, S. Amigoni, F. Guittard, *Adv. Mater*., 2013, **25**, 1378.

5 a) A. B. D. Cassie, S. Baxter, *Trans. Faraday Soc*., 1944, **40**, 546; b) A. Lafuma, D. Quéré, *Nat. Mater*., 2003, **2**, 457; c) Y. K. Lai, X. F. Gao, H. F. Zhuang, J. Y. Huang, C. J. Lin, L. Jiang, *Adv. Mater*., 2009, **21**, 3799.

6 a) D. L. Tian, J. Zhai, Y. L. Song, L. Jiang, *Adv. Funct. Mater*., 2011, **21**, 4519; b) H. Mertaniemi, V. Jokinen, L. Sainiemi, S. Franssila, A. Marmur, O. Ikkala, R. H. A. Ras, *Adv. Mater*., 2011, **23**, 2911; c) Q. F Cheng, L. Jiang, Z. Y Tang, *Acc. Chem. Res.* 2014, **47**, 1256−1266.

7 a) G. M. Gong, J. T. Wu, J. G. Liu, N. Sun, Y. Zhao, L. Jiang, *J. Mater. Chem*., 2012, **22**, 8257; b) L. Zhai, F. C. Cebeci, R. E. Cohen, M. F. Rubner, *Nano Lett*., 2004, **4**, 1349; c) J. Zimmermann, F. A. Reifler, G. Fortunato, L. C. Gerhardt, S. Seeger, *Adv. Funct. Mater.*, 2008, **18**, 3662.

8 a) T. Verho, C. Bower, P. Andrew, S. Franssila, O. Ikkala, R. H. A. Ras, *Adv. Mater.*, 2011, **23**, 673; b) A. Checco, A. Rahman, C. T. Black, *Adv. Mater.*, 2014, **26**, 886; c) L. Bocquet, E. Lauga, *Nat. Mater.*, 2011, **10**, 334.

9 X. Deng, L. Mammen, H. J. Butt, D. Vollmer, *Science*, 2012, **335**, 67.

10 X. Deng, L. Mammen, Y. F. Zhao, P. Lellig, K. Müllen, C. Li, H. J. Butt, D. Vollmer, *Adv. Mater.*, 2011, **23**, 2962.

11 P. A. Levkin, F. Svec, J. M. J. Fréchet, *Adv. Funct. Mater*., 2009, **19**, 1993.

12 a) Y. Li, F. Liu, J. Q. Sun, *Chem*. *Commun*., 2009, 2730; b) Q. F. Xu, J. N. Wang, K. D. Sanderson, *ACS Nano*, 2010, **4**, 2201; c) Y. Gahmawan, L. Xu, S. Yang, *J. Mater. Chem. A*, 2013, **1**, 2955; d) K.C. Park, H. J. Choi, C. H. Chang, R. E. Cohen, G. H. Mckinley, G. Barbastathis, *ACS Nano*, 2012, **6**, 3789.

13 a) Y. K. Lai, Y. X. Tang, J. J. Gong, D. G. Gong, L. F. Chi, C. J. Lin, Z. Chen, *J*. *Mater*. *Chem*., 2012, **22**, 7420; b) T. Wang, T. T. Isimjan, J. F. Chen, S. Rohani, *Nanotechnology*, 2011, **22**, 265708; c) S. Kato, A. Sato, *J. Mater. Chem.*, 2012, 22, 8613; d) R. G. Karunakaran, C.-H. Lu, Z. Zhang, S. Yang, *Langmuir*, 2011, **27**, 4594.

14 a) J. A. Hiller, J. D. Mendelsohn, M. F. Rubner, *Nat. Mater.*, 2002, **1**, 59; b) Y. F. Li, J. H. Zhang, S. J. Zhu, H. P. Dong, F. Jia, Z. H. Wang, Z. Q. Sun, L. Zhang, Y. Li, H. B. Li, W. Q. Xu, B. Yang, *Adv. Mater.*, 2009, **21**, 4731; c) L. Yao, J. H. He, *Chin. J. Chem.*, 2014, **32,** 507.

15 a) R. B. Pernites, R. R. Ponnapati, R. C. Advincula, *Adv*. *Mater*., 2011, **23**, 3207; b) L. B. Xu, W. Chen, A. Mulchandani, Y. S. Yan, *Angew*. *Chem*. *Int*. *Ed*., 2005, **44**, 6009; c) M. Nicolas, F. Guittard, S. Géribaldi, *Angew. Chem*., 2006, **118**, 2309.

16 a) W. J. Hong, Y. X. Xu, G. W. Lu, C. Li, G. Q. Shi, *Electrochem*. *Commun*., 2008, **10,** 1555; b) D. DeLongchamp, P. T. Hammond, *Adv*. *Mater*., 2001, **13**, 1455.

17 a) Z. X. Xue, M. J. Liu, L. Jiang, *J. Polym*. *Sci*. *part B*: *Polym*. *Phys*., 2012, **50**, 1209; b) A. K. Kota, Y. X. Li, J. M. Mabry, A. Tuteja, *Adv*. *Mater*., 2012, **24**, 5837; c) J. Zhang, S. Seeger, *Angew*. *Chem*. *Int*. *Ed.*, 2011, **50**, 6652.

18 a) Q.-S. Zheng, Y. Yu, Z.-H. Zhao, *Langmuir*, 2005, **21**, 12207; b) Q. F. Xu, B. Mondal, A. M. Lyons, *ACS Appl. Mater. Interfaces*, 2011, **3**, 3508.